batteries

MDPI

Supplementary Materials

Functionalization of Cathode–Electrolyte Interface with Ionic Liquids for High-Performance Quasi-Solid-State Lithium–Sulfur Batteries: A Low-Sulfur Loading Study

Milinda Kalutara Koralalage [1,†], Varun Shreyas [2,†], William R. Arnold [2], Sharmin Akter [2], Arjun Thapa [3], Badri Narayanan [2,3,*], Hui Wang [2,3], Gamini U. Sumanasekera [1,3,*] and Jacek B. Jasinski [3,*]

[1] Department of Physics and Astronomy, University of Louisville, Louisville, KY 40292, USA
[2] Department of Mechanical Engineering, University of Louisville, Louisville, KY40292, USA
[3] Conn Center for Renewable Energy Research, University of Louisville, Louisville, KY 40292, USA
* Correspondence: badri.narayanan@louisville.edu (B.N.); gamini.sumanasekera@louisville.edu (G.U.S.); jacek.jasinski@louisville.edu (J.B.J.)
† These authors contributed equally to this work.

2.6. Battery Assembly

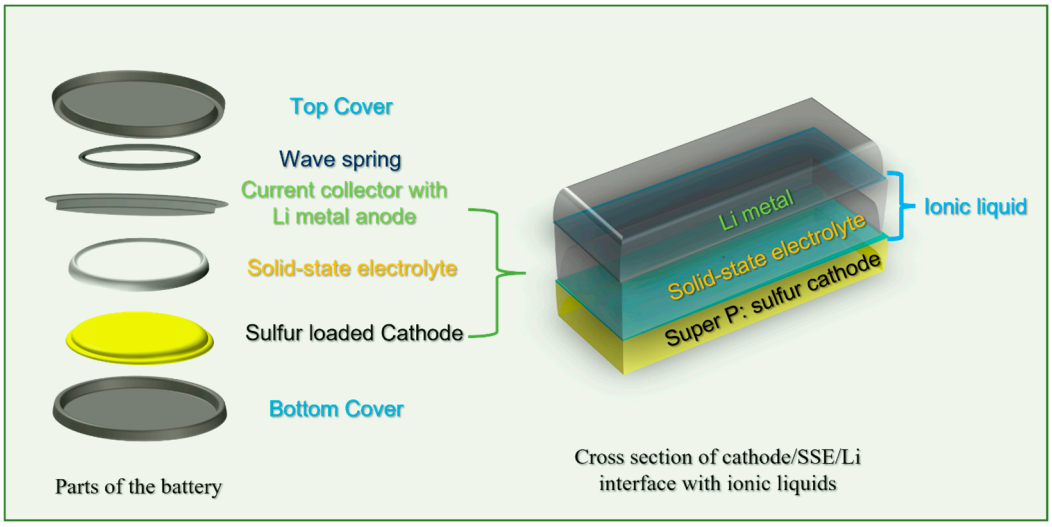

Figure S1: Parts of the CR2032 coin cell assembly and cross section of cathode/SSE/Li metal interface with thin layer of ionic liquids.

Figure S1 shows the essential parts of a CR2032 battery used to assemble QSSEB and the cross-sectional view of the QSSEB cathode/SSE/Li metal interface in the presence of ILs at cathode/SSE and Li/SSE interfaces.

3.2. Electrochemical Testing

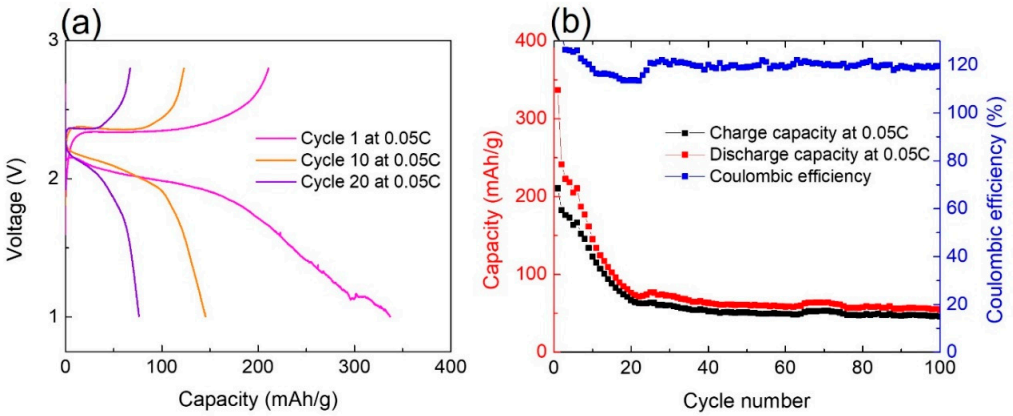

Figure S2: Performance of QSSEB with ionic liquid LiTFSI(1M) in PYR.

Figure S2 (a) & (b) show the performance of QSSEB with the ionic liquid LiTFSI (1M) dissolved in PYR at C/20 rate for 100 cycles. Voltage profile is shown during charging and discharging at cycles 1, 10, and 20.

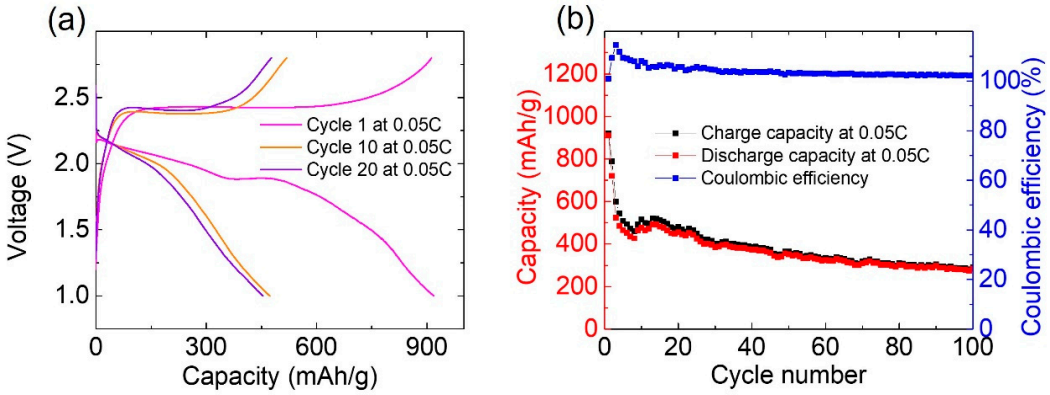

Figure S3: Performance of QSSEB with ionic liquid LiTFSI (1M) in PYR:DOL (1:1).

Figure S3 (a) & (b) show the performance of QSSEB with the ionic liquid LiTFSI(1M) dissolved in PYR:DOL(1:1) at C/20 rate for 100 cycles. Voltage profile is shown during charging and discharging at cycles 1, 10, and 20.

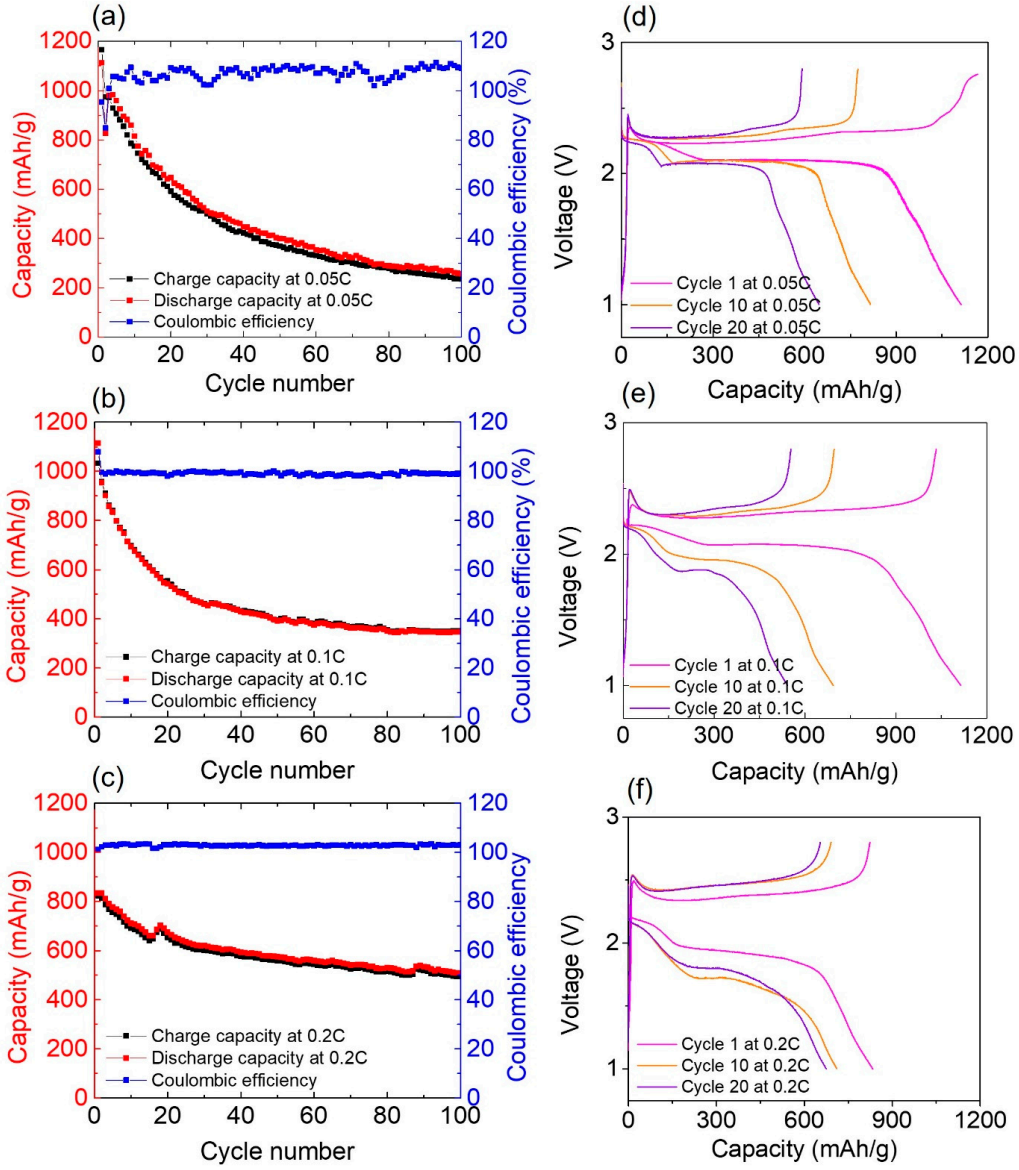

Figure S4: C rate dependent cyclic performance at (a) C/20, (b) C/10, (c) C/5 rates and charge discharge curves at (d) C/20, (e) C/10, (f) C/5 for batteries consist of SP-S/SSE/Li with 40 µl of IL LiTFSI(2M) PYR:DOL(1:1).

Figure S4 (a), (b) & (c) show the C rate dependent Capacity (left axis) and coulombic efficiency (right axis) versus cycle number while Figure S3 (d), (e) & (f) show the discharge and charge profiles (at cycles 1, 10 and 20. Batteries charged/discharged at C/20 (Figure S4 (a) & (d)) and C/10 (Figure S4 (b) & (e)) showed initial discharge capacity of ~ 1100 mAh/g. They both seem to retain the capacity > 300 mAh/g after 100 cycles but the battery tested at C/10 showed better coulombic efficiency. However, the battery tested at C/5 showed initial capacity of ~800 mAh/g and retained above 60% of initial capacity of ~500 mAh/g after 100 cycles with stable coulombic efficiency (Figure S4 (c) &(f)).

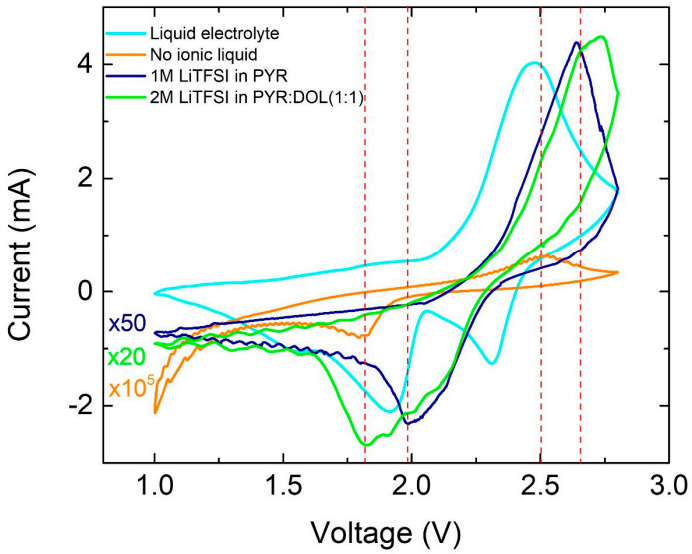

Figure S5: Cyclic voltammogram for batteries with and without ionic liquids.

Figure S5 shows the cyclic voltammograms recorded for batteries *consisting of SP-S/SSE/Li* (i) without ionic liquid (orange line), (ii) with IL 1M LiTFSI in PYR (dark blue line) and (iii) with 2M LiTFSI in PYR:DOL(1:1) (Green line) in comparison to liquid electrolyte Li-S battery (light blue line). Third cycle of cyclic voltammograms for each battery is plotted with the magnifications indicated.

3.3. XPX Analysis

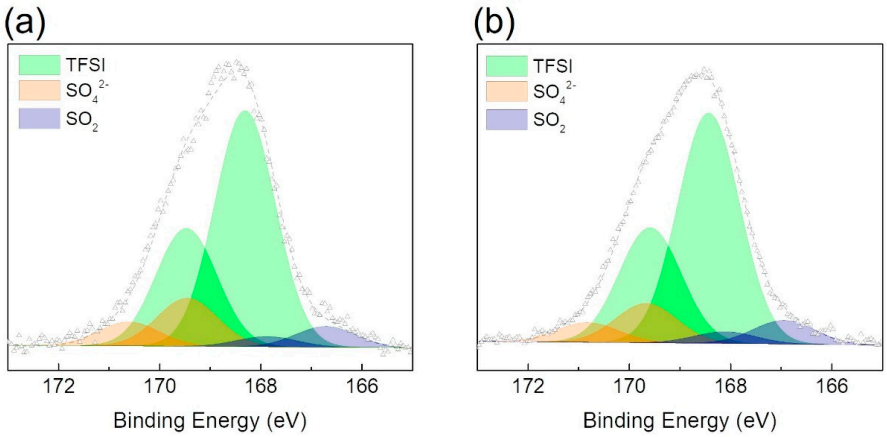

Figure S6: XPS S2p high BE peak of the cathode-SSE interface of 2 batteries containing (a) LiTFSI(1M) in PYR and (b) LiTFSI(2M) in PYR:DOL (1:1) after discharge of 100 cycles.

Figure S6 shows the XPS S2p high BE peak of the cathode-SSE interface of 2 batteries containing (a) LiTFSI (1 M) in PYR and (b) LiTFSI (2 M) in PYR:DOL(1:1) after 100 cycle discharge. Both spectra could be fitted with three peaks with each peak consisting, both $S2p_{1/2}$ and $S2p_{3/2}$ components due to spin-orbit splitting (energy spacing, Δ=1.16eV, intensity ratio=0.511). Both samples show dominant peaks corresponding to TFSI anion from LiTFSI and PYR14-TFSI. Peaks corresponding to SO_2 were detected presumably due to the decomposition of TFSI anions in both LiTFSI and PYR14-TFSI. There are additional peaks

related to sulfates (SO_4^{2-}) presumably due to the reaction of sulfides with any residual oxygen.

3.4. AIMD Simulation Results

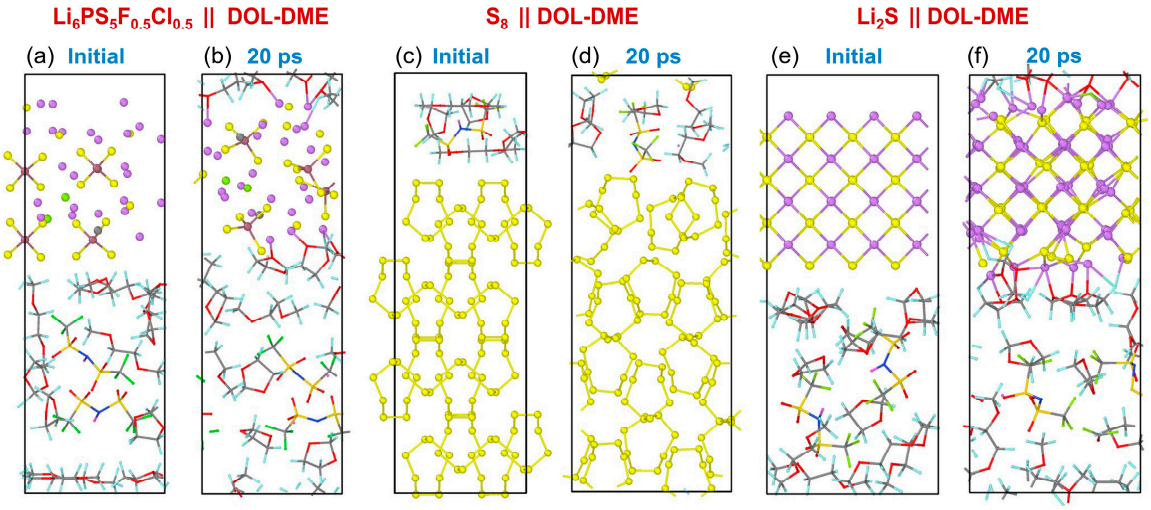

Figure S7: Structural evolution of DOL:DME (1:1) interface with (a) $Li_6PS_5F_{0.5}Cl_{0.5}$, (b) S_8, and (c) Li_2S obtained from ab initio molecular dynamics simulations under ambient conditions.

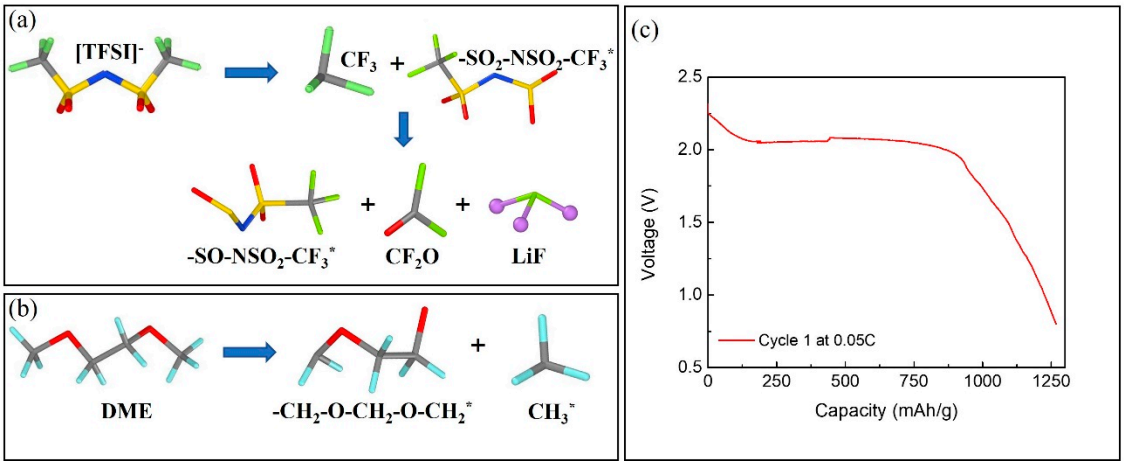

Figure S8: The decomposition sequence of (a) $[TFSI]^-$ and (b) DME molecules for DOL:DME (1:1) interface with Li_2S obtained from ab initio molecular dynamics simulations under ambient conditions (* represents the complexes), and (c) discharge curve of DOL:DME (1:1) IL based battery which did not charge back.

Figure S8 shows the decomposition sequence of (a) $[TFSI]^-$ and (b) DME molecules for DOL:DME (1:1) interface with Li_2S obtained from AIMD simulations under ambient conditions (* represents the complexes), and (c) discharge curve of DOL:DME (1:1) IL based battery which did not charge back.